Kinetic Modeling of the Liquid-Phase Hydrogenation of Cinnamaldehyde on Copper-Based Catalysts

Alberto J. Marchi, José F. Paris, Nicolás M. Bertero, and Carlos R. Apesteguía*

Catalysis Science and Engineering Research Group (GICIC), Instituto de Investigaciones en Catálisis y Petroquímica−INCAPE−(UNL−CONICET), Santiago del Estero 2654, (3000) Santa Fe, Argentina

The liquid-phase hydrogenation of cinnamaldehyde (CAL) on copper-based catalysts was studied using pseudo-homogeneous and heterogeneous Langmuir−Hinshelwood−Hougen−Watson (LHHW) kinetics. Three catalysts were used: Cu/SiO_2, which was prepared via incipient wetness impregnation, and Cu−Al and Cu−Zn−Al, which were obtained by coprecipitation. The pattern observed for the activity and selectivity to cinnamyl alcohol (COL) was as follows: Cu−Zn−Al > Cu−Al > Cu/SiO_2. The best fitting, using LHHW models, was obtained, in all the cases, by assuming total surface coverage. However, and consistent with pseudo-homogeneous analysis, the best fitting for the Cu/SiO_2 and Cu−Al was achieved by considering that CAL is much more strongly adsorbed than products on metal copper sites to yield essentially hydrocinnamaldehyde (HCAL). In contrast, the best fitting for the Cu−Zn−Al catalyst was obtained by considering that (i) the adsorption strength values of CAL, HCAL, and COL on the catalyst surface are similar; and (ii) CAL is adsorbed on two different types of active sites (specifically, CAL adsorbs on Cu^0 to form HCAL and on the $Cu-Zn^{2+}$ interface sites to produce essentially COL). The modeling of catalytic data using LHHW kinetics and the estimated parameters allowed for interpretation of the reasons for the higher COL formation rate observed on Cu−Zn−Al catalyst, in comparison to Cu/SiO_2 and Cu−Al catalysts.

1. Introduction

Unsaturated alcohols obtained via the hydrogenation of α,β-unsaturated aldehydes are valuable chemical intermediates for the synthesis of fine chemicals, especially those used in pharmacology, perfumery, and the food-processing industry. However, the selective hydrogenation of α,β-unsaturated aldehydes to the corresponding unsaturated alcohols is not easily achieved on noble-metal-based catalysts, because hydrogenation of the conjugated C═C bond is thermodynamic and kinetically favored, in comparison to that of the C═O group.[1] Different approaches have been attempted to modify the intrinsic catalytic properties of noble metals and increase the selectivity to unsaturated alcohols. For example, some authors proposed the addition of a second component forming bimetallic compounds,[2,3] whereas others studied the catalyst modification by adding metal cations[4,5] or using different types of supports.[6,7]

On the other hand, several authors have studied the kinetic modeling of hydrogenation of α,β-unsaturated aldehydes on noble-metal-based catalysts, both in the liquid phase and the gas phase.[8−12] Neri et al.[8] used Ru/Al_2O_3 and $Ru-Sn/Al_2O_3$ catalysts for cinnamaldehyde (CAL) hydrogenation, and they determined that the best fitting for the experimental results was obtained through the use of Langmuir−Hinshelwood−Hougen−Watson (LHHW) models involving one and two active sites, respectively. The model also assumed that all the surface reactions are rate-determining, while adsorption−desorption steps are in quasi-equilibrium. Authors interpreted these results by considering that only Ru metal sites are active on Ru/Al_2O_3, whereas an additional active site is generated when tin is added to the same catalyst. Vergunst et al.[11] modeled the hydrogenation of cinnamaldehyde on monolithic Pt/C catalysts and observed that the best approximation was obtained when using a one-site model that considers that the elementary steps involved in the reaction network (i.e., surface reactions and adsorption−desorption steps) are all rate-controlling. An important feature for the kinetic modeling of α,β-unsaturated aldehydes is whether the adsorption of hydrogen is competitive or not with the adsorption of reactants and products. For liquid-phase hydrogenation of citral on platinum-based catalysts, Singh and Vannice[9] proposed that hydrogen and citral are adsorbed on the same type of active site. A similar assumption was considered by Chang et al.[10] to interpret the catalytic results obtained for ketone hydrogenation over Raney nickel catalysts. In contrast, Vergunst et al.[11] reported that, for cinnamaldehyde hydrogenation on Pt/C catalysts, the adsorption of hydrogen on platinum was not competitive. Besides, it must be noted that strong catalyst−sorbate interactions can occur during the hydrogenation reaction and should be taken into account for the development of the corresponding kinetic model.[12]

In a previous work,[13] we reported that ternary Cu−Zn−Al catalysts are ∼1 order of magnitude more active than Cu/SiO_2 for cinnmaldehyde hydrogenation and produce predominantly cinnamyl alcohol. We explained the superior performance of Cu−Zn−Al catalysts by the presence of surface Cu^0-Zn^{2+} sites that efficiently catalyze the cinnamyl alcohol formation from cinnmaldehyde via a dual-site reaction pathway. In this work, we have extended our studies on the liquid-phase hydrogenation of CAL on copper-based catalysts by performing a kinetic modeling of the experimental results using LHHW-type models. Basically, we tested different LHHW models that were developed to cover the following alternative reaction pathways in the reaction mechanism: (a) the presence of one or two types of active sites; (b) the strong adsorption of reactants and/or products on the catalyst surface; (c) total covering of the catalytic surface; and (d) both competitive and noncompetitive H_2 adsorption.

* To whom correspondence should be addressed. Tel.: 54-342-4555279. Fax: 54-342-4531068. E-mail address: capesteg@fiqus.unl.edu.ar.

10.1021/ie070305n CCC: $37.00
Published on Web 07/21/2007

Table 1. Characterization of the Catalysts Used in This Work

	XRD analysis						
		Mixed Oxide Crystallite Size (Å)		Physical Properties			
catalyst	hydrated precursor	spinel	CuO	surface area, S_g (m^2/g)	pore volume, V_p (cm^3/g)	CuO reduction peak,[a] T_m (K)	H_2 uptake[b] (cm^3/g)
Cu/SiO_2	$Cu(NO_3)_2$		275	218	0.78	610	0.322
Cu−Al	amorphous			230	0.48	582	0.936
Cu−Zn−Al	hydrotalcite	47		221	0.46	575	1.507

[a] Determined from temperature-programmed reduction (TPR) experiments. [b] Strongly held hydrogen.

2. Experimental Section

A Cu/SiO_2 catalyst (SiO_2, Grace 62, 99.7%) was prepared via incipient wetness impregnation via the dropwise addition of an aqueous solution of $Cu(NO_3)_2 \cdot 3H_2O$ with a copper concentration of 0.6 M. The impregnated sample was dried at 353 K overnight and then decomposed in N_2 at 673 K for 4 h. Hydrated precursors of binary Cu−Al and ternary Cu−Zn−Al catalysts were prepared by coprecipitation, as described in details elsewhere.[14,15] An acidic solution of the metal nitrates was contacted with an aqueous solution of K_2CO_3 at a constant pH of 7. The two solutions were simultaneously added dropwise to 400 mL of distilled water that was maintained at a temperature of 333 K in a stirred batch reactor. The resulting precipitates were aged for 2 h at 333 K in their mother liquor and then filtered, washed thoroughly with deionized water at 333 K, and dried at 353 K overnight. Dried precipitates were decomposed overnight in nitrogen at 773 K to obtain the corresponding mixed oxides. The potassium content was <0.1 wt %, which confirmed that K^+ ions were effectively removed by filtration and washing of the precipitated precursors. In all the samples, the copper loading was in the range of 12−13 wt %. The (Cu + Zn)/Al and Zn/Al ratios for the ternary Cu−Zn−Al sample were 1 and 0.75, respectively, which, on a spinel-like basis, results in a $[CuO]_{0.5} \cdot [ZnO]_{0.5} \cdot ZnAl_2O_4$ formula.

Temperature-programmed reduction (TPR) experiments were performed in a Okhura TPD 20025 unit, using a 5% H_2/Ar gaseous mixture at 60 cm^3/min STP. The sample size was 150 mg. Samples were heated from 298 K to 873 K at a rate of 10 K/min. Because water was formed during the sample reduction, the gas exiting from the reactor was passed through a cold trap before entering the thermal conductivity detector.

Hydrogen chemisorption was measured via volumetric adsorption experiments at room temperature in a conventional vacuum apparatus. Catalysts were reduced in H_2 at 473 K for 1 h and then outgassed at the same temperature under a vacuum of 10^{-7} bar. After cooling to room temperature, a first isotherm was drawn for measuring the total H_2 uptake. Then, and after 1 h of evacuation at room temperature, a second isotherm was performed to determine the amount of weakly adsorbed H_2. The amount of strongly chemisorbed H_2 was calculated as the difference between total and weakly adsorbed H_2. The pressure range of isotherms was 0−0.15 bar and extrapolation to zero pressure was used as a measure of the gas uptake on copper.

The crystalline structures of the samples were determined via X-ray diffraction (XRD), in the 2θ range of 10°−80°, using a Shimadzu XD-D1 diffractometer and nickel-filtered Cu Kα radiation. Brunauer−Emmett−Teller (BET) surface areas (S_g) and pore volumes (V_p) of mixed oxides were measured by N_2 physisorption at its boiling point in a NOVA-1000 sorptometer (Quantochrome Corporation). Elemental compositions were measured using atomic absorption spectroscopy (AAS).

The liquid-phase hydrogenation of CAL was studied in a Parr model 4563 reactor, with a total volume of 600 mL, at 393 K and 10 bar, and using 2-propanol as the solvent. The autoclave was loaded with 150 mL of solvent, 10 mL of CAL, and 1 g of catalyst. Prior to catalytic tests, samples were activated ex situ in flowing hydrogen (30 mL/min) at 473−523 K for 1 h and then transferred to the reactor, avoiding contact with air. Afterward, the reaction system was heated to 393 K at a rate of 2 K/min. The pressure then was rapidly increased to 10 bar with H_2. The concentration evolutions with time of unreacted CAL and reaction products were followed by ex situ gas chromatography, using a Varian Star 3400 CX chromatograph that was equipped with a flame ionization detector, temperature programmer, and a 30 m Carbowax Amine capillary column. Samples from the reaction system were taken using a loop under pressure, to avoid flushing. Data were collected every 15−30 min for 250−500 min. The conversion of cinnamaldehyde (X_{CAL}, given in terms of the number of moles of cinnmaldehyde reacted per mole of citral fed) was calculated as

$$X_{CAL} = \frac{C^0_{CAL} - C_{CAL}}{C^0_{CAL}}$$

where C^0_{CAL} is the initial concentration of citral and C_{CAL} is the concentration of cinnamaldehyde at reaction time t. The selectivities (S_i, given in terms of the number of moles of product i per mole of cinnamaldehyde reacted) were calculated as

$$S_i\,(\%) = \frac{C_i \times 100}{\sum C_i}$$

where C_i is the concentration of product i. It was determined that stirrer speeds of >500 rpm and particle sizes of <100 μm were sufficient to ensure no influence of diffusion limitations on the reaction kinetic.

3. Catalyst Characterization

The crystalline phases of hydrated precursors and mixed oxides were determined using the XRD technique (see Table 1). No crystalline phases were detected for the coprecipitated Cu−Al sample. XRD patterns showed a single crystalline phase with a hydrotalcite structure for Cu−Zn−Al, which consisted of layered double hydroxides with brucite-like layers and a $[(\Sigma Me^{2+})_{1-x}Al_x(OH)_2]^{x+}(CO_3)^{2-}_{x/2} \cdot mH_2O$ composition, where Me = Cu or Zn. The stoichiometric hydrotalcite structure—$(\Sigma Me^{2+})_6Al_2(OH)_{16}CO_3.mH_2O$—is reached when $x = 0.25$ (according to ASTM Standard 14-191).

Thermal decomposition of hydroxycarbonate Cu−Al and Cu−Zn−Al precursors led to the formation of mixed oxides with high surface area and large pore volume (see Table 1). In the case of the Cu−Zn−Al sample, the intimate contact between the Cu, Zn, and Al cations in the hydrotalcite structure is preserved during decomposition and leads to the formation of well-mixed mixed oxides.[16] The specific surface area of the Cu/

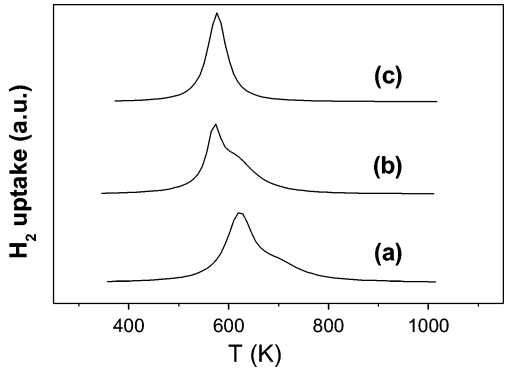

Figure 1. Temperature-programmed reduction (TPR) profiles of copper-based samples: (a) Cu/SiO_2, (b) Cu−Al, and (c) Cu−Zn−Al. Heating rate = 10 K/min.

Scheme 1

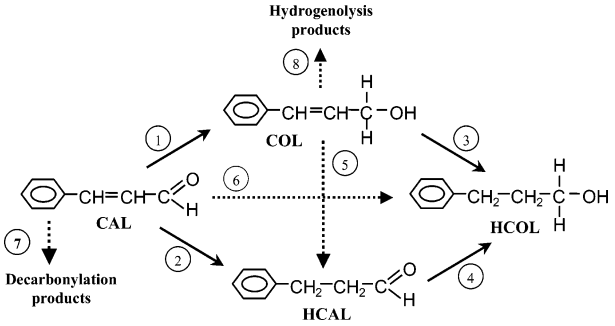

SiO_2 sample was similar to those of mixed oxides prepared by coprecipitation (see Table 1).

XRD patterns of the hydrated precursors after decomposition in N_2 at 773 K showed that Cu/SiO_2 contain a single crystalline phase of CuO (ASTM Standard 5-0661) with large crystallite size (see Table 1), whereas binary Cu−Al is a quasi-amorphous sample. The ternary Cu−Zn−Al sample showed diffraction patterns that were consistent with the presence of a spinel-like phase (ASTM Standard 5-0669). No segregation of CuO or ZnO crystalline phases were detected in the Cu−Zn−Al mixed oxide, thereby indicating that both cations are highly dispersed in the spinel-like matrix.

TPR profiles of the hydrated precursors after decomposition in N_2 at 773 K are shown in Figure 1. The Cu/SiO_2 sample exhibits a broad peak, with a maximum at 610 K (see Table 1) that results from the reduction of CuO.[17] Similarly, TPR traces of the Cu−Al and Cu−Zn−Al samples show only single CuO reduction peaks, but the peak maxima are shifted to lower temperatures (590 and 570 K, respectively), compared to that of Cu/SiO_2. No evidence of $CuAl_2O_4$ formation was detected in the Cu−Al and Cu−Zn−Al samples, which is consistent with XRD characterization. Bulk $CuAl_2O_4$ spinel is thermodynamically unstable at <873 K;[18] however, the formation of $CuAl_2O_4$ surface spinels that contain the Cu^{2+} ions in a distorted octahedral geometry has been observed at much lower temperatures.[19]

The metallic fraction of the catalysts was characterized by hydrogen chemisorption at room temperature. Prior to the volumetric adsorption experiments, samples were reduced in pure H_2 at 473 K for 1 h. Hydrogen chemisorption data then would be essentially related to the reduced copper fraction of the catalysts. The results are shown in Table 1. The hydrogen uptake increased in the order

$$Cu/SiO_2 < Cu-Al < Cu-Zn-Al$$

which reflects the increase of the metallic copper dispersion from the Cu/SiO_2 sample to the ternary Cu−Zn−Al sample. This result is in complete agreement with the TPR characterization data previously shown.

In summary, the characterization results showed that the samples described in Table 1 present similar textural properties, but different structural and surface properties. Unreduced Cu/SiO_2 contains large CuO crystallites with a tenorite-like structure. After reduction with H_2, large Cu^0 particles, presenting very low interaction with the SiO_2 support, are formed. The Cu−Zn−Al sample contains CuO very well-dispersed in a nonstoichiometric zinc aluminate-like phase. Treatment with hydrogen at 473 K completely reduces the CuO to metallic copper, forming very small Cu^0 particles that are highly interdispersed in a nonstoichiometric spinel phase. The high dispersion of small Cu^0 crystallites in the spinel matrix favors the generation of surface $Cu-Zn^{2+}$ dual sites.[20] An intermediate situation regarding both metal crystallite size and metal−support interaction should be expected for the binary Cu−Al sample.

4. Catalytic Results

Cinnamaldehyde hydrogenation on the copper-based catalysts described in Table 1 formed essentially cinnamyl alcohol (COL), hydrocinnamaldehyde (HCAL), and hydrocinnamyl alcohol (HCOL). The evolution of CAL conversion and product selectivities with reaction time for all the catalysts are shown in Figure 2. The CAL conversion rate on the ternary Cu−Zn−Al sample was significantly higher than that on the Cu−Al and Cu/SiO_2 samples. In fact, after 5 h of reaction, CAL was totally consumed on the Cu−Zn−Al sample, but the X_{CAL} values were only ∼0.4 and ∼0.6 on the Cu/SiO_2 and Cu−Al samples, respectively. Figure 2 also shows that X_{CAL} increased linearly with time on the Cu−Al and Cu/SiO_2 samples but not on the Cu−Zn−Al sample, thereby suggesting that cinnamaldehyde is transformed following different reaction rate expressions.

Product selectivities in Figure 2 show that, at the begining of the reaction, only COL and HCAL produced directly from cinnamaldehyde are formed. Both COL and HCAL reach maxima selectivities as they are converted to HCOL in consecutive hydrogenations, but maximal values are reached faster for COL than for HCAL, particularly on the Cu−Zn−Al sample. The zero initial slope of the HCOL selectivity curve is consistent with its formation via the secondary hydrogenation of primary COL and HCAL products. The HCOL formation rate is clearly higher on the Cu−Zn−Al catalyst than on the Cu−Al and Cu/SiO_2 catalysts. On the other hand, the Cu/SiO_2 and Cu−Al samples hydrogenated cinnamaldehyde mainly to HCAL, thereby showing that they selectively catalyze the hydrogenation of C═C bonds. In contrast, the Cu−Zn−Al sample formed initially similar amounts of COL and HCAL. As expected, at high X_{CAL}, the selectivity toward HCOL, which is the terminal product in the reaction network, increased on all the catalysts.

5. Reaction Kinetics Modeling: Pseudo-Homogeneous Model

To determine the hydrogenation kinetic constants using heterogeneous models, we initially performed a kinetic study by modeling catalytic data using a pseudo-homogeneous model to obtain more details of the reactions involved in the CAL hydrogenation mechanism. The reaction network for CAL hydrogenation is potentially a complex combination of series

Table 2. Reaction Kinetics Modeling Using the Pseudo-Homogeneous Model Described by eqs 1−4[a]

number of parameters (k_1, k_2, k_3, k_4)	estimates	confidence interval[b]	Reaction Orders μ	Reaction Orders ν	coefficient of determination, r^2	model selection criterion, MSC	k_1/k_2 ratio
			Cu/SiO_2 Catalyst				
4	$k_3 < 0$	NS	0	0	0.985	6.0	0.12
3 ($k_3 = 0$)	**all positives**	**S**	**0**	**0**	**0.999**	**5.6**	**0.20**
4	$k_3 < 0$	NS	1	1	0.998	5.1	0.17
3 ($k_3 = 0$)	all positives	S	1	1	0.998	5.1	0.23
			Cu−Al Catalyst				
4	all positives	NS	0	0	0.999	6.2	0.37
3 ($k_4 = 0$)	**all positives**	**S**	**0**	**0**	**0.999**	**5.9**	**0.80**
4	all positives	NS	1	1	0.998	5.2	0.52
3 ($k_3 = 0$)	all positives	S	1	1	0.998	5.3	0.61
			Cu−Zn−Al Catalyst				
4	all positives	NS	0	0	0.970	1.84	0.85
3 ($k_4 = 0$)	all positives	NS	0	0	0.971	1.88	1.60
4	all positives	S	1	1	0.996	4.2	1.08
4	$k_4 < 0$	NS	1	2	0.998	5.3	0.46
4	**all positives**	**S**	**2**	**1**	**0.999**	**5.6**	**2.60**
4	all positives	NS	2	2	0.997	4.7	1.17

[a] The best agreement between the experimental data and the model predictions is denoted in bold. [b] NS = all or some of the left limits are negative at 95% confidence or less; S = the left limits are all positive at 95% confidence or more.

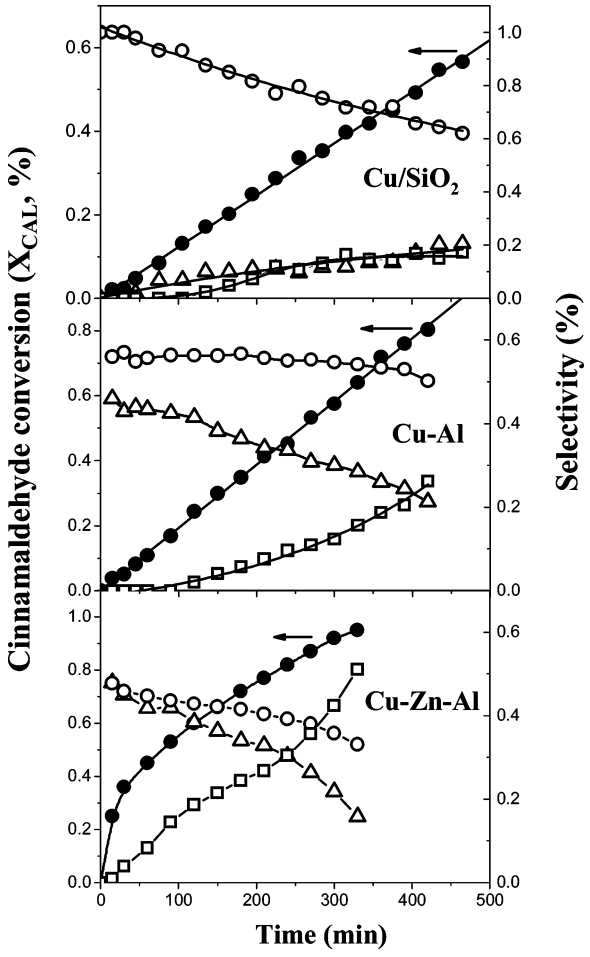

Figure 2. Cinnamaldehyde conversion and product selectivities for cinnamaldehyde hydrogenation reactions on copper-based catalysts [393 K, 10 bar, 1 g catalyst]: (○) HCAL, (△) COL, and (□) HCOL.

and parallel reactions that, based on the results shown in Figure 2 and previous literature,[2,21,22] can be depicted as shown in Scheme 1. However, when the reaction is performed in the liquid phase on copper-based catalysts, the reaction system becomes relatively simple. In fact, as it can be inferred from the results in Figure 2, reactions 7 and 8 in Scheme 1 can be considered to be negligible, because we did not detect formation of any COL hydrogenolysis or CAL decarbonylation products. The direct hydrogenation of CAL to HCOL (reaction 6) is also not included for modeling, because our results in Figure 2 clearly show that HCOL is not formed from the direct hydrogenation of CAL. Thus, the hydrogenation of CAL to HCAL and COL, and that of HCAL and COL to HCOL, seem to be the only significant reaction pathways on copper-based catalysts (shown as the solid lines in Scheme 1). The kinetics of CAL conversion reactions is represented then by the following differential equations system, which includes the CAL conversion rate and the formation rates of COL, HCAL, and HCOL:

$$r_{CAL} = -\frac{dC_{CAL}}{dt} = k_1(C_{CAL})^{\mu} + k_2(C_{CAL})^{\nu} \quad (1)$$

$$r_{COL} = \frac{dC_{COL}}{dt} = k_1(C_{CAL})^{\mu} - k_3C_{COL} - k_5C_{COL} \quad (2)$$

$$r_{SAL} = \frac{dC_{HCAL}}{dt} = k_2(C_{CAL})^{\nu} - k_4C_{HCAL} + k_5C_{COL} \quad (3)$$

$$r_{SOL} = \frac{dC_{HCOL}}{dt} = k_3C_{COL} + k_4C_{HCAL} \quad (4)$$

Here, μ and ν are the reactions orders, with respect to CAL, for CAL hydrogenation to COL and to HCAL, respectively. Reaction orders that are equal to one are assumed for both the hydrogenation of COL and HCAL to HCOL and the isomerization of COL to HCAL, based on data obtained on copper-based catalysts by other authors.[23,24]

The system of differential equations was solved numerically using the Runge−Kutta−Merson algorithm. The model parameter estimation was performed by nonlinear regression, using a Levenberg−Marquardt algorithm, which minimizes the objective function:

$$S = \sum (C_{i,t}^{exp} - C_{i,t}^{calc})^2 \quad (5)$$

where C^{exp} and C^{calc} are the experimental and calculated concentrations, respectively, i is the chemical compound, and t is the reaction time.

The model adequacy and the discrimination between models were determined using the model selection criterion (MSC), according to eq 6:

$$\mathrm{MSC} = \ln\left[\frac{\sum_{i=1}^{n}(y_{\mathrm{exp}_i} - \bar{y}_{\mathrm{exp}})^2}{\sum_{i=1}^{n}(y_{\mathrm{exp}_i} - y_{\mathrm{calc}_i})^2}\right] - \frac{2p}{n} \quad (6)$$

where n is the number of experimental data; p is the amount of parameters fitted; and y_{calc} and y_{exp} the predicted and the experimental values, respectively. When various different models are compared, the most significant is that which leads to the highest MSC value.

The coefficient of determination (r^2) gives the fitting quality (i.e., the percentage of explanation of the total data variation around the average observed value) and was calculated using eq 7:

$$r^2 = \frac{(y_{\mathrm{calc}_i} - \bar{y}_{\mathrm{exp}})^2}{(y_{\mathrm{exp}_i} - \bar{y}_{\mathrm{exp}})^2} \quad (7)$$

The results of reaction kinetic modeling using the pseudo-homogeneous model are shown in Table 2. The best agreement between the experimental data and the model predictions (high values of r^2 and MSC, positive estimates, and positive left limits at 95% confidence or more) was obtained by assuming that (i) the kinetic constant for COL isomerization to HCAL is negligible ($k_5 = 0$) for all the catalysts; (ii) the reactions orders are $\mu = 0$ and $\nu = 0$ on the Cu/SiO_2 and Cu−Al samples, and $\mu = 2$ and $\nu = 1$ on the Cu−Zn−Al sample. We also included in Table 2 the obtained k_1/k_2 ratios that reflect the initial COL/HCAL selectivity ratios in Scheme 1. It is observed that the k_1/k_2 ratio on the Cu−Zn−Al sample is 10 times higher than that on the Cu/SiO_2 sample and a similar qualitative difference is reflected in the values obtained on the same catalysts for the initial COL/HCAL selectivity ratios (see Figure 2).

6. Reaction Kinetics Modeling: Heterogeneous Model

The experimental data of Figure 2 and the results obtained using the pseudo-homogeneous model show that the copper-based catalysts used in this work may be divided in two groups following their catalytic performances: (a) the Cu/SiO_2 and Cu−Al catalysts present a low activity to transform CAL, and hydrogenate preferentially the C═C bond, exhibiting high selectivities to HCAL (reaction orders, with respect to CAL, for CAL conversion to HCAL and COL are zero on both catalysts); and (b) the Cu−Zn−Al catalyst shows a high activity for converting CAL and produces significant amounts of COL by selectively hydrogenating the C═O group of the CAL molecule (reaction orders, with respect to CAL, are 2 and 1 for CAL conversion to COL and HCAL, respectively).

These catalytic and kinetic differences may be explained by considering the different catalyst surface and structural properties. Cu−Al and Cu/SiO_2 catalysts contained large crystals of metallic copper that strongly adsorb CAL and favor its hydrogenation to HCAL. Strong reactant adsorption on metallic copper was also consistent with the observed zero-order reaction in CAL on the Cu−Al and Cu/SiO_2 catalysts. In contrast, the metallic copper phase in the Cu−Zn−Al sample is highly dispersed and strongly interacts with a nonstoichiometric Zn_x-Al_2O_{3+x} spinel-like phase. The close interaction between Cu^0 and Zn^{2+} ions of the spinel-like phase favors the formation of Cu^0−Zn^{2+} dual sites that preferentially adsorb CAL on Zn^{2+} via its C═O group, which is then selectively hydrogenated by hydrogen chemisorbed dissociatively on neighboring Cu^0 sites. This explains the observed higher formation rate of COL on the Cu−Zn−Al sample, with respect to the Cu−Al and Cu/SiO_2 samples.

Based on the results previously discussed, we considered here the following hypothesis for the formulation of LHHW heterogeneous models:

(1) CAL can be adsorbed on the Cu−Zn−Al catalyst on both metallic (M) and cationic (L) sites.

(2) CAL can be converted to COL on both M and L sites, whereas HCAL is produced only on M sites.

(3) COL and HCAL are hydrogenated to HCOL over M sites.

(4) HCOL is not adsorbed on the catalyst surface.

(5) Hydrogen adsorption may be either competitive or noncompetitive.

(6) Reactant and product adsorption/desorption steps are all reversible quasi-equilibrium steps.

(7) Hydrogenation surface reactions are all rate-determining steps.

(8) Because of the high H_2 partial pressure that is applied, hydrogenation surface reactions are all irreversible.

(9) Hydrogen concentration in the fluid phase is constant, because of the constant hydrogen partial pressure during the entire experiment, the high solvent volume, and efficient mixing.

Considering the former hypothesis with active sites M and L, and noncompetitive H_2 chemisorption (hydrogen adsorbed on metallic site S), the elementary steps shown in eqs 8−18 represent the general reaction mechanism:

$$\mathrm{H_2} + 2\mathrm{S} \rightleftarrows 2\mathrm{H{-}S} \qquad (K_{\mathrm{HS}} = (C_{\mathrm{HS}})^2/[(C_{\mathrm{S}})^2 p_{\mathrm{H_2}}]) \quad (8)$$

$$\mathrm{CAL} + \mathrm{L} \rightleftarrows \mathrm{CAL\text{-}L} \qquad (K_{\mathrm{CALL}} = C_{\mathrm{CALL}}/(C_{\mathrm{L}} C_{\mathrm{CAL}})) \quad (9)$$

$$\mathrm{CAL} + \mathrm{M} \rightleftarrows \mathrm{CAL\text{-}M} \qquad (K_{\mathrm{CALM}} = C_{\mathrm{CALM}}/(C_{\mathrm{M}} C_{\mathrm{CAL}})) \quad (10)$$

$$\mathrm{CAL\text{-}L} + 2\mathrm{H{-}S} \rightarrow \mathrm{COL\text{-}L} + 2\mathrm{S} \qquad (r_{11} = k_{11} C_{\mathrm{CALL}} (C_{\mathrm{HS}})^2) \quad (11)$$

$$\mathrm{COL\text{-}L} \rightleftarrows \mathrm{COL} + \mathrm{L} \qquad (K_{\mathrm{COLL}} = C_{\mathrm{L}}/(C_{\mathrm{L}} C_{\mathrm{COL}})) \quad (12)$$

$$\mathrm{CAL\text{-}M} + 2\mathrm{H{-}S} \rightarrow \mathrm{COL\text{-}M} + 2\mathrm{S} \qquad (r_{12} = k_{12} C_{\mathrm{CALM}} (C_{\mathrm{HS}})^2) \quad (13)$$

$$\mathrm{COL\text{-}M} \rightleftarrows \mathrm{COL} + \mathrm{M} \qquad (K_{\mathrm{COLM}} = C_{\mathrm{COLM}}/(C_{\mathrm{M}} C_{\mathrm{COL}})) \quad (14)$$

$$\mathrm{CAL\text{-}M} + 2\mathrm{H{-}S} \rightarrow \mathrm{HCAL\text{-}M} + 2\mathrm{S} \qquad (r_2 = k_2 C_{\mathrm{CALM}} (C_{\mathrm{HS}})^2) \quad (15)$$

$$\mathrm{HCAL\text{-}M} \rightleftarrows \mathrm{HCAL} + \mathrm{M} \qquad (K_{\mathrm{HCALM}} = C_{\mathrm{HCALM}}/(C_{\mathrm{M}} C_{\mathrm{HCAL}})) \quad (16)$$

$$\text{COL-M} + 2\text{H}-\text{S} \rightarrow \text{HCOL} + \text{M} + 2\text{S} \qquad (r_3 = k_3 C_{\text{COLM}} (C_{\text{HS}})^2) \quad (17)$$

$$\text{HCAL-M} + 2\text{H}-\text{S} \rightarrow \text{HCOL} + \text{M} + 2\text{S} \qquad (r_4 = k_4 C_{\text{HCALM}} (C_{\text{HS}})^2) \quad (18)$$

The general system of differential equations to be solved, based on eqs 8−18, is

$$\frac{dC^*_{\text{CAL}}}{dt} = \frac{1}{C^0_{\text{CAL}}}\frac{dC_{\text{CAL}}}{dt} = -\frac{1}{C^0_{\text{CAL}}}(r_{11} + r_{12} + r_2) = -r^*_{11} + r^*_{12} - r^*_2 \quad (19)$$

$$\frac{dC^*_{\text{HCAL}}}{dt} = \frac{1}{C^0_{\text{CAL}}}\frac{dC_{\text{HCAL}}}{dt} = \frac{1}{C^0_{\text{CAL}}}(r_2 - r_4) = r^*_2 - r^*_4 \quad (20)$$

$$\frac{dC^*_{\text{HCOL}}}{dt} = \frac{1}{C^0_{\text{CAL}}}\frac{dC_{\text{HCOL}}}{dt} = \frac{1}{C^0_{\text{CAL}}}(r_3 + r_4) = r^*_3 + r^*_4 \quad (21)$$

$$\frac{dC^*_{\text{COL}}}{dt} = \frac{1}{C^0_{\text{CAL}}}\frac{dC_{\text{COL}}}{dt} = \frac{1}{C^0_{\text{CAL}}}(r_{11} + r_{12} - r_3) = r^*_{11} + r^*_{12} - r^*_3 \quad (22)$$

where $C^*_i = C_i/C^0_{\text{CAL}}$ is the relative concentration of compound i and $r^*_j = r_j/C^0_{\text{CAL}}$ is the modified reaction rate corresponding to reaction j.

Considering the catalytic results analyzed previously for CAL hydrogenation on different copper-based catalysts, we initially proposed and analyzed the following five models:

Model I: It is represented by the reaction mechanism described for the elementary steps described by eqs 8−18 and the corresponding rate expressions given in the Appendix (eqs I-4−I-8).

Model II: Same as Model I, but now competitive chemisorption of H_2 is assumed; i.e., the step described by eq 8 becomes

$$\text{H}_2 + 2\text{M} \leftrightarrow 2\ \text{H.M} \quad \left(K_{\text{H M}} = \frac{(C_{\text{HM}})^2}{(C_{\text{M}})^2 p_{\text{H}_2}}\right) \qquad (8b)$$

Model III: This model assumes that CAL is adsorbed only on M sites to give COL and HCAL; i.e., the steps described by eqs 9, 11, and 12 do not happen.

Model IV: Same as Model III, but now H_2 chemisorption is assumed to be competitive.

Model V: Same as Model III, but now the adsorption of CAL is assumed to be much stronger than the adsorption of COL and HCAL; i.e., $K_{\text{CAL}} \gg K_{\text{COL}}$ and K_{HCAL}.

6.1. Cu/SiO$_2$ Catalyst. Models I and II were not considered for the Cu/SiO_2 sample, because this sample does not contain L sites. Calculations using Models III, IV, and V showed that only Model V gave an acceptable fitting, according to both statistical and physical point of views. In fact, some of the estimates for Models III and IV were negative and all the parameter confidence intervals had a negative left limit within 95% confidence. The LHHW expressions involved in Model V are shown below in eqs 23−26 and are obtained from the equation set that represents the general reaction mechanism (eqs I.4−I.8 in the Appendix) by considering the strong adsorption of CAL (i.e., $K_{\text{CALM}} \gg K_{\text{HCALM}}$, K_{COLM}) and that r^*_{11} does not exist (the catalyst does not contain L sites).

$$r^*_{12} = \frac{k_{12} C^{\text{T}}_{\text{M}} (C^{\text{T}}_{\text{S}})^2 K_{\text{HS}} p_{\text{H}_2}}{C^0_{\text{CAL}} (1 + \sqrt{K_{\text{H S}} p_{\text{H}_2}})^2} = k^*_{12} \quad (23)$$

$$r^*_2 = \frac{k_2 C^{\text{T}}_{\text{M}} (C^{\text{T}}_{\text{S}})^2 K_{\text{HS}} p_{\text{H}_2}}{C^0_{\text{CAL}} (1 + \sqrt{K_{\text{HS}} p_{\text{H}_2}})^2} = k^*_2 \quad (24)$$

$$r^*_3 = \frac{k_3 C^{\text{T}}_{\text{M}} (C^{\text{T}}_{\text{S}})^2 K_{\text{HS}} p_{\text{H}_2} K_{\text{COLM}} C^*_{\text{COL}}}{C^0_{\text{CAL}} (1 + \sqrt{K_{\text{HS}} p_{\text{H}_2}})^2 K_{\text{CALM}} C^*_{\text{CAL}}} = k^*_3 \frac{C^*_{\text{COL}}}{C^*_{\text{CAL}}} \quad (25)$$

$$r^*_4 = \frac{k_4 C^{\text{T}}_{\text{M}} (C^{\text{T}}_{\text{S}})^2 K_{\text{HS}} p_{\text{H}_2} K_{\text{HCALM}} C^*_{\text{HCAL}}}{C^0_{\text{CAL}} (1 + \sqrt{K_{\text{HS}} p_{\text{H}_2}})^2 K_{\text{CALM}} C^*_{\text{CAL}}} = k^*_4 \frac{C^*_{\text{HCAL}}}{C^*_{\text{CAL}}} \quad (26)$$

When the system of differential equations that is given as eqs 19−22 was solved by introducing the r^*_j expressions of eqs 23−26, we obtained a negative estimate for k^*_3. Recalculations using only three k^*_j kinetic constants, by considering either $k^*_3 = 0$ or $k^*_4 = 0$, are shown in Table 3. In both cases, Model V gave positive estimates and was significantly different from zero, even at 99% confidence for k^*_j values; however, the MSC value obtained by assuming $k^*_3 = 0$ was higher than that calculated for $k^*_4 = 0$. We then inferred that Model V with $k^*_3 = 0$ was the best model to interpret the catalytic data. Figure 3a shows the good agreement that was obtained between the experimental data and the predictions of Model V with $k^*_3 = 0$. On the other hand, the evolution of residuals ($C_{i,\text{exp}} - C_{i,\text{cal}}$) as a function of time (Figure 3b) followed a random trend, which is consistent with the hypothesis of random error included in nonlinear regression used for parameter estimations and gives additional support to the model adequacy. The k^*_{12}, k^*_2, and k^*_4 estimates and the corresponding confidence intervals at 95% confidence are shown in Table 4, to compare with the similar kinetic parameters determined for the Cu−Al and Cu−Zn−Al catalysts. The $k^*_{12}/(k^*_{12} + k^*_2)$ ratio obtained from Table 4 was ~0.16, which reflects the fact that the Cu/SiO_2 catalyst is much more active for hydrogenating the C═C bond than the C═O group of the CAL molecule. The good fitting obtained in Figure 3 by assuming $k^*_3 = 0$ shows that the C═C bond in COL is much more difficult to be hydrogenated than the C═O bond in CAL, whereas the fact that k^*_4 is significantly higher than k^*_{12} indicates that the C═O group in HCAL is much more easily hydrogenated than that in CAL. The relative values obtained for parameters k^*_{12}, k^*_2, and k^*_4 on the Cu/SiO_2 sample were in good agreement with those calculated using the pseudo-homogeneous model.

6.2. Cu−Al Catalyst. Similarly to the Cu/SiO_2 catalyst, the Cu−Al catalyst does not contain L sites and, as a consequence, Models I and II were discarded. Calculations using Model III resulted in an acceptable fitting of the experimental results, but all the parameters gave confidence intervals at 95% with a negative left extreme. Model IV that assumes competitive hydrogen chemisorption led to negative estimates for parameters K_{HCALM} and k^*_4. When parameters K_{HCALM} and k^*_4 were not considered (i.e., the steps described by eqs 16 and 18 were removed), then the estimates for the remaining six parameters resulted in positive values, but all of them had confidence intervals with negative left extremes at 95% confidence or less. Only calculations using the system of eqs 23−26 with Model V, which assumes that CAL is adsorbed on copper much stronger than COL or HCAL, gave a good fitting, from both

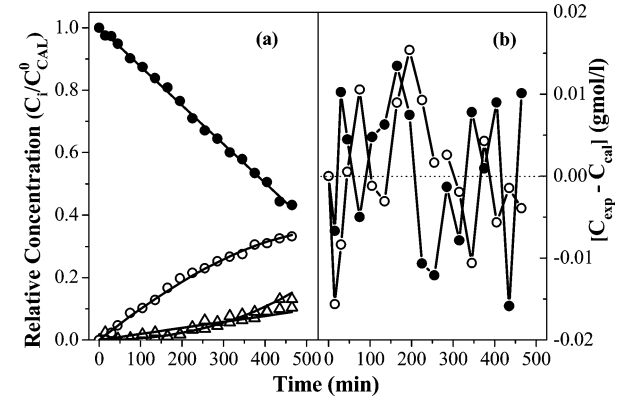

Figure 3. Cinnamaldehyde (CAL) hydrogenation on Cu/SiO_2: (a) experimental results (denoted by symbols) and modeling results (represented as full lines); (b) evolution of residuals for CAL and HCAL [393 K; 10 bar; Model V] ((○) HCAL, (△) COL, and (□) HCOL).

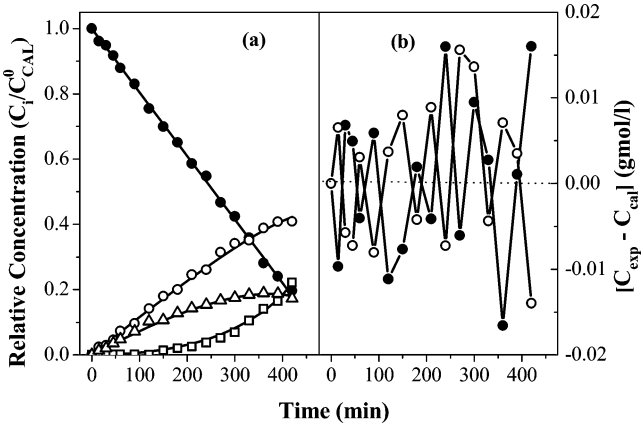

Figure 4. CAL hydrogenation on Cu−Al: (a) experimental results (denoted by symbols) and modeling results (represented as full lines); (b) evolution of residuals for CAL and HCAL [393 K; 10 bar; Model V] ((○) HCAL, (△) COL, and (□) HCOL).

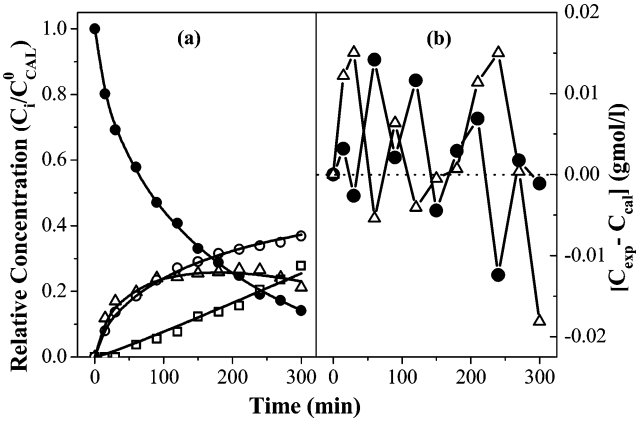

Figure 5. CAL hydrogenation on Cu−Al−Zn: (a) experimental results (denoted by symbols) and modeling results (represented as full lines); (b) evolution of residuals for CAL and COL [393 K; 10 bar; Model I] ((○) HCAL, (△) COL, and (□) HCOL).

physical and statistical point of views. Table 5 shows, in fact, that all the estimates were positive and significantly different from zero with a 95% confidence when the four k_j^* parameters involved in Model V were used to fit experimental results. The elimination of k_3^* or k_4^* from Model V led to a significant increase of the sum of squared deviations and lower values of parameters r^2 and SMC. These later results suggest that, on the Cu−Al catalyst, both COL and HCAL are converted to HCOL, in contrast to what was determined on the Cu/SiO_2 catalyst (on this catalyst, only HCAL was converted to HCOL). Figure 4a shows a good agreement between the experimental data and the Model V predictions when the relative concentrations of reactant and products are represented as functions of time. Besides, the distribution of residuals exhibits an acceptable random trend when represented as a function of time (see Figure 4b).

Table 3. Estimates and Statistics Determined at the 99% Confidence Level by Applying Model V to Experimental Values Obtained during the Liquid-Phase Hydrogenation of Cinnamaldehyde on a Cu/SiO_2 Catalyst at 393 K and 10 bar

		Confidence Intervals	
parameter	estimate	left limit	right limit
	$r^2 = 0.996$, MSC = 5.4		
k_{12}^*	3.53×10^{-4}	2.84×10^{-4}	4.23×10^{-4}
k_2^*	8.43×10^{-4}	7.93×10^{-4}	8.93×10^{-4}
k_3^*	2.10×10^{-3}	7.01×10^{-4}	3.50×10^{-3}
k_4^*	0		
	$r^2 = 0.998$, MSC = 6.7		
k_{12}^*	1.93×10^{-4}	1.65×10^{-4}	2.22×10^{-4}
k_2^*	1.03×10^{-3}	9.90×10^{-4}	1.07×10^{-3}
k_3^*	0		
k_4^*	8.82×10^{-4}	6.90×10^{-4}	1.08×10^{-3}

The kinetic parameters for CAL hydrogenation on the Cu−Al catalyst obtained using Model V are shown in Table 4. The $k_{12}^*/(k_{12}^* + k_2^*)$ ratio was ∼0.4, which is significantly higher than that obtained on the Cu/SiO_2 catalyst (0.16) and reflects the fact that Cu−Al sample promotes the initial formation of COL from CAL more efficiently than the Cu/SiO_2 sample. Besides, the k_3^*/k_4^* ratio was ∼4.0 indicating that conversion of COL to HCOL is more rapid than the HCAL conversion to HCOL, which is opposite to the case observed with the Cu/SiO_2 sample. The relative values obtained for parameters k_{12}^*, k_2^*, k_3^*, and k_4^* were again in good agreement with those calculated using the pseudo-homogeneous model.

6.3. Cu−Zn−Al Catalyst. Models I−V were used to fit the experimental results obtained on a ternary Cu−Zn−Al catalyst. A reasonable fitting was observed when applying Model I. However, almost all of the confidence intervals, at 95% or less, had a negative left extreme. When it was assumed in Model I that COL is produced only via the hydrogenation of CAL adsorbed over L sites (i.e., the steps described by eqs 13 and 14 are not considered), a negative estimate for K_{HCALM} was obtained. On the other hand, removing K_{HCALM} and k_4^* did not result in any significant improvement. In contrast, when, in Model I, one assumed a total covering of active sites, noncompetitive hydrogen chemisorption, and no interaction of HCAL with the catalyst surface (i.e., $K_{HCALM} = 0$), a good fitting, with positive estimates, positive confidence interval extremes even at 99%, and high values of r^2 and MSC, was obtained, as shown in Table 6. Calculations using Model II, which assumes competitive hydrogen chemisorption, led to confidence intervals with a negative left extreme, even if K_{HCALM} and k_4^* are eliminated and a total covering is supposed to occur. On the other hand, negative estimates for some parameters, such as K_{HCALM} and k_4^*, were obtained using Models III and IV, which assume that the hydrogenation of CAL to HCAL and COL occurs only on M sites. Removing K_{HCALM} and k_4^* did not improve the goodness of fit, because some confidence intervals showed a negative left extreme. In the case of Model IV, which considers competitive hydrogen chemisorption, the estimate for K_{HM} was negative, which might be interpreted as if the step described by eq 8b does not happen. Finally, Model V, which

Table 4. Parameters Estimated with a 95% Confidence by Applying Modified Model V and Model I to Experimental Values Obtained for CAL Hydrogenation over Copper-Based Catalysts at 393 K and 10 bar

	Modified Model V		Modified Model I
parameter	Cu/SiO_2	Cu−Al	Cu−Zn−Al
k_{11}^* (min^{-1})			$2.10 \times 10^{-2} \pm 9.6 \times 10^{-3}$
k_{12}^* (min^{-1})	$1.93 \times 10^{-4} \pm 1.9 \times 10^{-5}$	$7.77 \times 10^{-4} \pm 4.8 \times 10^{-5}$	
k_2^* (min^{-1})	$1.05 \times 10^{-3} \pm 3.0 \times 10^{-5}$	$1.17 \times 10^{-3} \pm 4 \times 10^{-5}$	$1.41 \times 10^{-2} \pm 3.6 \times 10^{-3}$
k_3^* (min^{-1})		$1.13 \times 10^{-3} \pm 2.3 \times 10^{-4}$	$9.31 \times 10^{-4} \pm 6.1 \times 10^{-5}$
k_4^* (min^{-1})	$9.90 \times 10^{-4} \pm 1.3 \times 10^{-4}$	$2.80 \times 10^{-4} \pm 1.2 \times 10^{-4}$	
K_{COLL}^*			25.4 ± 13.5
K_{COLM}^*			21.6 ± 6.9

assumes that K_{CALM} is much higher than the other adsorption constants, gave a very poor approximation of the experimental data.

Taking into account the previously discussed results, Model I, which was modified by assuming a total covering of M and L active sites and no adsorption of HCAL, was selected as the best model among Models I−V to describe the liquid-phase hydrogenation of CAL over the Cu−Zn−Al catalyst. The LHHW expressions for this model are shown in eqs 27−29 and are obtained from the equation set that represents the general reaction mechanism (see eqs I.4−I.8 in the Appendix) by considering (i) $K_{HCALM} \approx 0$, (ii) total site coverage (i.e., the concentration of vacant sites is negligible), and (iii) the hydrogenation of CAL to COL occurs only on L sites (i.e., reaction r_{12}^* does not occur).

$$r_{11}^* = \frac{k_{11} C_L^T (C_S^T)^2 K_{CALL} K_{HS} p_{H_2} C_{CAL}^*}{C_{CAL}^0 (1 + \sqrt{K_{HS} p_{H_2}})^2 (K_{CALL} C_{CAL}^* + K_{COLL} C_{COL}^*)} = \frac{k_{11}^* C_{CAL}^*}{C_{CAL}^* + K_{COLL}^* C_{COL}^*} \quad (27)$$

$$r_2^* = \frac{k_2 C_M^T (C_S^T)^2 K_{CALM} K_{HS} p_{H_2} C_{CAL}^*}{C_{CAL}^0 (1 + \sqrt{K_{HS} p_{H_2}})^2 (K_{CALM} C_{CAL}^* + K_{COLM} C_{COL}^*)} = \frac{k_2^* C_{CAL}^*}{C_{CAL}^* + K_{COLM}^* C_{COL}^*} \quad (28)$$

$$r_3^* = \frac{k_3 C_M^T (C_S^T)^2 K_{COLM} K_{HS} p_{H_2} C_{COL}^*}{C_{CAL}^0 (1 + \sqrt{K_{HS} p_{H_2}})^2 (K_{CALM} C_{CAL}^* + K_{COLM} C_{COL}^*)} = \frac{k_3^* C_{COL}^*}{C_{CAL}^* + K_{COLM}^* C_{COL}^*} \quad (29)$$

where

$$K_{COLL}^* = \frac{K_{COLL}}{K_{CALL}}$$

and

$$K_{COLM}^* = \frac{K_{COLM}}{K_{CALM}}$$

Figure 5a shows that a very good agreement is verified between the experimental data and the Model I predictions. As a matter of fact, the differences between the experimental values and the Model I predictions were always $< 2 \times 10^{-2}$, which corresponds to a relative residual of 5% or less. Furthermore, these residuals showed an acceptable random behavior (see Figure 5b). The kinetic parameter values determined using the modified Model I, which involves the system of eqs 27−29, are given in Table 4. The $k_{11}^*/(k_{11}^* + k_2^*)$ ratio was ~0.6 and reflects the fact that the Cu−Zn−Al catalyst exhibited the highest initial selectivity to COL among the copper-based catalysts analyzed in this work. Parameter k_3^* was 1 order of magnitude less than k_{11}^* and k_2^*, indicating that, on the Cu−Zn−Al sample, the COL conversion rate to HCOL is significantly lower than the CAL conversion rate to COL and HCAL. In contrast to what was observed on the Cu/SiO_2 sample, HCAL was not hydrogenated to HCOL on the Cu−Zn−Al sample. The relative values obtained for parameters k_{11}^*, k_2^*, and k_3^* were in good agreement with those calculated from the pseudo-homogeneous model.

In summary, the best model to interpret the CAL hydrogenation results obtained on the Cu−Zn−Al catalyst considers that CAL interacts with the catalyst surface via two different type of active sites: one (metallic M site) essentially interacts with the C═C bond, whereas the other (cationic L site) preferentially activates the C═O group of CAL molecules. Furthermore, the model assumes that dissociative hydrogen adsorption occurs on metallic S sites and is not competitive with CAL, COL, and HCAL adsorptions.

6.4. Comparison of Catalysts. Although parameters k_j^* (for $j = 11, 12, 2, 3, 4$) in Models I−V are actually groups of different constants, it should be noted that they are proportional to the respective kinetic constant k_j, as shown in eqs 23−26, and therefore may be used to interpret the catalyst activity and selectivity data. For example, a comparison of the $k_{11}^*(k_{12}^*)/k_2^*$ values calculated from Table 4 gives the following pattern for the selectivity to COL:

$$Cu-Zn-Al > Cu-Al > Cu/SiO_2$$

In other words, considering the best LHHW model for every catalyst, it is possible to predict the pattern of catalyst selectivity to COL for the liquid-phase hydrogenation of CAL.

The value of k_{12}^* was significantly higher on the Cu−Al catalyst than on the Cu/SiO_2 catalyst (see Table 4), but k_2^* was similar on both catalysts, thereby indicating that both the initial CAL conversion rate and the initial selectivity to COL are higher on the Cu−Al catalyst than on the Cu/SiO_2 catalyst. This result also shows that the higher COL selectivity observed on the Cu−Al catalyst is not due to a decrease in the conversion rate of CAL to HCAL but rather to an increase in the CAL hydrogenation rate to COL. Similarly, the values of $k_{11}^*(k_{12}^*)/k_2^*$ obtained from Table 4 predict that both the initial selectivity to COL and the initial conversion rate of CAL will be higher on the Cu−Zn−Al catalyst, in comparison to the Cu−Al or Cu/SiO_2 catalysts.

Finally, the LHHW-like models predict a different behavior for the interaction between the catalyst surface and the product

Table 5. Estimates and Statistics Determined at the 99% Confidence Level by Applying Model V to Experimental Values Obtained during the Liquid-Phase Hydrogenation of Cinnamaldehyde on a Cu−Al Catalyst at 393 K and 10 bar

		Confidence Intervals	
parameter	estimate	left limit	right limit
Number of Parameters = 43, $r^2 = 0.996$, MSC = 7.1			
k_{12}^*	7.77×10^{-4}	7.29×10^{-4}	8.25×10^{-4}
k_2^*	1.17×10^{-3}	1.13×10^{-3}	1.22×10^{-3}
k_3^*	1.13×10^{-3}	8.99×10^{-4}	1.36×10^{-3}
k_4^*	2.80×10^{-4}	1.60×10^{-4}	3.99×10^{-4}
Number of Parameters = 3, $r^2 = 0.988$, MSC = 6.5			
k_{12}^*	8.65×10^{-4}	8.26×10^{-4}	9.04×10^{-4}
k_2^*	1.08×10^{-3}	1.05×10^{-3}	1.11×10^{-3}
k_3^*	1.48×10^{-3}	1.24×10^{-3}	1.71×10^{-3}
k_4^*	0		
Number of Parameters = 3, $r^2 = 0.989$, MSC = 5.5			
k_{12}^*	5.67×10^{-4}	5.20×10^{-4}	6.15×10^{-4}
k_2^*	1.36×10^{-3}	1.30×10^{-3}	1.42×10^{-3}
k_3^*	0		
k_4^*	6.86×10^{-4}	5.01×10^{-4}	8.70×10^{-4}

Table 6. Estimates and Statistics Determined at the 99% Confidence Level by Applying Modified Model 1 to Experimental Values Obtained during the Liquid-Phase Hydrogenation of Cinnamaldehyde on a Cu−Zn−Al Catalyst at 393 K and 10 bar[a]

		Confidence Intervals	
parameter	estimate	left limit	right limit
k_{COLL}^*	21.2	7.8	34.5
k_{COLM}^*	20.5	12.0	28.9
K_{HCALM}	0		
k_{11}^*	1.78×10^{-2}	8.5×10^{-3}	2.71×10^{-2}
k_2^*	1.33×10^{-2}	9.0×10^{-3}	1.76×10^{-2}
k_3^*	9.37×10^{-4}	8.55×10^{-4}	1.02×10^{-3}

[a] Note: $r^2 = 0.999$, MSC = 6.3.

molecules. For example, both COL and HCAL are expected to be hydrogenated to HCOL on the Cu−Al catalyst, whereas selective HCAL hydrogenation would occur on the Cu/SiO_2 catalyst, and only COL would be hydrogenated to HCOL on the Cu−Zn−Al catalyst.

7. Conclusions

Kinetic Langmuir−Hinshelwood−Hougen−Watson (LHHW)-like models that satisfactorily interpret the experimental data obtained on Cu/SiO_2, Cu−Al, and Cu−Zn−Al catalysts for the liquid-phase hydrogenation of cinnmaldehyde were developed, and these models are in good agreement with results obtained using pseudo-homogeneous models. For example, the best heterogeneous model for the Cu/SiO_2 and Cu−Al catalysts considers that cinnmaldehyde is adsorbed on metallic copper sites much stronger than cinnamyl alcohol and hydrocinnamaldehyde, in agreement with the fact that the best fit using pseudo-homogeneous models is obtained by assuming an order of zero in cinnmaldehyde. Also, the best heterogeneous model for the Cu−Zn−Al catalyst considers that cinnmaldehyde is adsorbed on two different types of active sites, to give cinnamyl alcohol and hydrocinnamaldehyde, respectively, which is consistent with the fact that the best pseudo-homogeneous model assumes an order of two, with respect to cinnmaldehyde.

Furthermore, the LHHW-type models developed in this work predict and explain, with physical meaning, the patterns of selectivity and activity experimentally determined on the Cu−Zn−Al, Cu−Al, and Cu/SiO_2 catalysts for cinnmaldehyde hydrogenation. Specifically, differences in catalyst activity and selectivity are interpreted by differences in both the nature of the active sites and the resulting reactant−active-site interaction. The kinetic modeling based on the set of elementary steps of the reaction mechanism resulting from this interpretation leads to a very good agreement with the experimental data.

Appendix. Rate Expressions

The LHHW-type expressions obtained for the general reaction mechanism represented in the text by eqs 8−18 (Model I) are given below (as eqs I.4−I.8), considering the site balances of eqs I.1−I.3. Model I assumes that three different type of sites are active on the catalyst surface (M, L, S) and that hydrogen chemisorption is not competitive with the adsorption of other reactants and products.

$$C_S^T = C_S + C_{HS} \tag{I.1}$$

$$C_L^T = C_L + C_{CALL} + C_{COLL} \tag{I.2}$$

$$C_M^T = C_M + C_{CALM} + C_{COLM} + C_{HCALM} \tag{I.3}$$

$$r_{11}^* = \frac{k_{11} C_L^T (C_S^T)^2 K_{CALL} K_{HS}\, p_{H_2} C_{CAL}^*}{C_{CAL}^0 \left(1 + \sqrt{K_{HS} p_{H_2}}\right)^2 \left[1 + \sum (K_{iL} C_i^*)\right]} \tag{I.4}$$

$$r_{12}^* = \frac{k_{12} C_M^T (C_S^T)^2 K_{CALM} K_{HS}\, p_{H_2} C_{CAL}^*}{C_{CAL}^0 \left(1 + \sqrt{K_{HS} p_{H_2}}\right)^2 \left[1 + \sum (K_{iM} C_i^*)\right]} \tag{I.5}$$

$$r_2^* = \frac{k_2 C_M^T (C_S^T)^2 K_{CALM} K_{HS} p_{H_2} C_{CAL}^*}{C_{CAL}^0 \left(1 + \sqrt{K_{HS} p_{H_2}}\right)^2 \left[1 + \sum (K_{iM} C_i^*)\right]} \tag{I.6}$$

$$r_3^* = \frac{k_2 C_M^T (C_S^T)^2 K_{COLM} K_{HS} p_{H_2} C_{COL}^*}{C_{CAL}^0 \left(1 + \sqrt{K_{HS} p_{H_2}}\right)^2 \left[1 + \sum (K_{iM} C_i^*)\right]} \tag{I.7}$$

$$r_4^* = \frac{k_2 C_M^T (C_S^T)^2 K_{HCALM} K_{HS} p_{H_2} C_{HCAL}^*}{C_{CAL}^0 \left(1 + \sqrt{K_{HS} p_{H_2}}\right)^2 \left[1 + \sum (K_{iM} C_i^*)\right]} \tag{I.8}$$

where

$$\sum (K_{iL} C_i^*) = K_{CALL} C_{CAL}^* + K_{COLL} C_{COL}^*$$

and

$$\sum (K_{iM} C_i^*) = K_{CALM} C_{CAL}^* + K_{COLM} C_{COL}^* + K_{HCALM} C_{HCAL}^*$$

Model III considers that the catalyst contains only two types of active sites (S, M) and that hydrogen chemisorption is not competitive with the adsorption of other reactants and products. The LHHW rate expressions for Model III are obtained by suppressing eqs I.2 and I.4 from the equation set previously given.

In Model II, the hydrogen chemisorption is competitive with the adsorption of other reactants and products. Then, in this model, eq. I.1 is suppressed and the site balance is given by eqs I.2 and I.9. The LHHW expressions for Model II are those represented by eqs I.10−I.14.

$$C_M^T = C_M + C_{CALM} + C_{COLM} + C_{HCALM} + C_{HM} \quad \text{(I.9)}$$

$$r_{11}^* = \frac{k_{11} C_L^T (C_M^T)^2 K_{CALL} K_{HM} p_{H_2} C_{CAL}^*}{C_{CAL}^0 \left[1 + \sqrt{K_{HM} p_{H_2}} + \sum (K_{iM} C_i^*)\right]^2 \left[1 + \sum (K_{iL} C_i^*)\right]} \quad \text{(I.10)}$$

$$r_{12}^* = \frac{k_{12} (C_M^T)^3 K_{CALM} K_{HM} p_{H_2} C_{CAL}^*}{\left[1 + \sqrt{K_{HM} p_{H_2}} + \sum (K_{iM} C_i^*)\right]^3} \quad \text{(I.11)}$$

$$r_2^* = \frac{k_2 (C_M^T)^3 K_{CALM} K_{HM} p_{H_2} C_{CAL}^*}{\left[1 + \sqrt{K_{HM} p_{H_2}} + \sum (K_{iM} C_i^*)\right]^3} \quad \text{(I.12)}$$

$$r_3^* = \frac{k_3 (C_M^T)^3 K_{COLM} K_{HM} p_{H_2} C_{COL}^*}{\left[1 + \sqrt{K_{H\,M} p_{H_2}} + \sum (K_{iM} C_i^*)\right]^3} \quad \text{(I.13)}$$

$$r_4^* = \frac{k_4 (C_M^T)^3 K_{HCALM} K_{HM} p_{H_2} C_{HCAL}^*}{\left[1 + \sqrt{K_{HM} p_{H_2}} + \sum (K_{iM} C_i^*)\right]^3} \quad \text{(I.14)}$$

Acknowledgment

We thank the Universidad Nacional del Litoral (UNL), Consejo Nacional de Investigaciones Científicas y Técnicas (CONICET), and Agencia Nacional de Promoción Científica y Tecnológica (ANPCyT), Argentina, for the financial support of this work.

Nomenclature

C_i = concentration of species i (mol/L)
C_i^* = relative concentration; $C_i^* = C_i/C_{CAL}^0$
L = Lewis sites
M, S = metal sites
C_L^T = concentration of total Lewis sites (mol/L)
C_M^T, C_S^T = concentration of total metal sites (mol/L)
C_L = concentration of vacant Lewis sites (mol/L)
C_M, C_S = concentration of vacant metal sites (mol/L)
C_{iL}, C_{iM}, C_{iS} = concentration of adsorbed species i (mol/L)
k_j = kinetic constant of reaction j
k_j^* = kinetic parameters defined in eqs 23−27
K_i = adsorption equilibrium constant
K_i^* = parameters defined in the text
r_j = reaction rate corresponding to reaction j (mol/(h L))
r_j^* = modified reaction rate; $r_j^* = r_j/C_{CAL}^0$ (h^{-1})
S_i = selectivity to product i (%)
t = reaction time (min)
X_{CAL} = conversion of cinnamaldehyde
r^2 = coefficient of determination
MSC = model selection criterion, as defined in eq 6

Greek Letters

ν, μ = reaction orders

Literature Cited

(1) Gallezot, P.; Richard, D. Selective Hydrogenation of α,β-Unsaturated Aldehydes. *Catal. Rev. Sci. Eng.* **1998**, *40*, 81.

(2) Englisch, M.; Ranade, V. S.; Lercher, J. A. Hydrogenation of Crotonaldehyde over Pt Based Bimetallic Catalysts. *J. Mol. Catal. A: Chem.* **1997**, *121*, 69.

(3) Yu, W.; Wang, Y.; Liu, H.; Zheng, W. Preparation and Characterization of Polymer-protected Pt/Co Bimetallic Colloids and their Catalytic Properties in the Selective Hydrogenation of Cinnamaldehyde *J. Mol. Catal. A: Chem*. **1996**, *112*, 105.

(4) Neri, G.; Mercadante, L.; Milone, C.; Pietropaolo, R.; Galvagno, S. Hydrogenation of Citral and Cinnamaldehyde over Bimetallic Ru-Me/Al_2O_3 Catalysts. *J. Mol. Catal. A: Chem*. **1996**, *108*, 41.

(5) Coloma, F.; Sepúlveda-Escribano, A.; García Fierro, J. L.; Rodríguez-Reinoso, F. Crotonaldehyde Hydrogenation over Bimetallic Pt-Sn Catalysts supported on Pregraphitized Carbon Black. Effect of the Preparation Method. *Appl. Catal., A* **1996**, *148*, 63.

(6) Blackmond, D. G.; Oukaci, R.; Blanc, B.; Gallezot, P. Geometric and Electronic Effects in the Selective Hydrogenation of α,β-Unsaturated Aldehydes over Zeolite-supported Metals. *J. Catal.* **1991**, *131*, 401.

(7) Da Silva, A. B.; Jordão, E.; Mendes, M. J.; Fouilloux, P. Effect of Metal-support Interaction during Selective Hydrogenation of Cinnamaldehyde to Cinnamyl Alcohol on Platinum-based Bimetallic Catalysts. *Appl. Catal., A* **1997**, *148*, 253.

(8) Neri, G.; Bonaccorsi, L.; Mercadante, L.; Galvagno, S. Kinetic Analysis of Cinnamaldehyde Hydrogenation over Alumina-Supported Ruthenium Catalysts. *Ind. Eng. Chem. Res.* **1997**, *36*, 3554.

(9) Singh, U. K.; Vannice, M. A. Influence of Metal−Support Interactions on the Kinetics of Liquid-Phase Citral Hydrogenation. *J. Mol. Catal. A: Chem.* **2000**, *163*, 233.

(10) Chang, N.-S.; Aldrett, S.; Holtzapple, M. T.; Davison, R. R. Kinetic Studies of Ketone Hydrogenation over Raney Nickel Catalyst. *Chem. Eng. Sci.* **2000**, *55*, 5721.

(11) Vergunst, Th.; Kapteijn, F.; Moulijn, J. A. Kinetics of Cinnamaldehyde Hydrogenation−Concentration-Dependent Selectivity. *Catal. Today* **2001**, *66*, 381.

(12) Zamostny, P.; Belohlav, Z. Identification of Kinetic Models of Heterogeneously Catalyzed Reactions. *Appl. Catal., A* **2002**, *225*, 29.

(13) Marchi, A. J.; Gordo, D. A.; Trasarti, A. F.; Apesteguía, C. R. Liquid Phase Hydrogenation of Cinnamaldehyde on Cu-based Catalysts. *Appl. Catal., A* **2003**, *249*, 53.

(14) Marchi, A. J.; Apesteguía, C. R. Impregnation-Induced Memory Effect of Thermally Activated Layered Double Hydroxides. *Appl. Clay Sci.* **1998**, *13*, 35.

(15) Ginés, M. J. L.; Marchi, A. J.; Apesteguía, C. R. Kinetic Study of the Reverse Water-gas Shift Reaction over CuO/ZnO/Al_2O_3 Catalysts. *Appl. Catal., A* **1997**, *154*, 155.

(16) Grandvallet, P.; Courthy, Ph.; Freund, E. In *Proceedings of the 8th International Congress on Catalysis*, Berlin, 1984; DECHEMA: Frankfurt, Germany, 1984; Vol. II, p 81.

(17) Ginés, M. J. L.; Apesteguía, C. R. Water-gas Shift Reaction: Reduction Kinetics and Mechanism of CuO/ZnO/Al_2O_3 Catalysts. In *Natural Gas Conversion VI: Proceedings of the 6th Natural Gas Conversion Symposium*, Girdwood, AK, June 17−22, 2001; Iglesia, E., Spivey, J. J., Fleisch, T. H., Eds.; Studies in Surface Science and Catalysis, Vol. 136; Elsevier, Amsterdam, 2001; p 447.

(18) Strohmeier, B. R.; Leyden, D. E.; Field, R. S.; Hércules, D. M. Surface Spectroscopic Characterization of Cu/Al_2O_3 Catalysts. *J. Catal*. **1985**, *94*, 514.

(19) Wolberg, A.; Roth, J. F. Copper Oxide Supported on Alumina: III. X-ray K-absorption Edge Studies of the Cu^{2+} Species. *J. Catal.* **1969**, *15*, 250.

(20) Hadden, R. A.; Sakakini, B.; Tabatabaei, J.; Waugh, K. C. Adsorption and Reaction Induced Morphological Changes of the Copper Surface of a Methanol Synthesis Catalyst. *Catal. Lett.* **1997**, *44*, 145.

(21) Augustine, R. L.; Meng, L. The Selective Hydrogenation of Unsaturated Aldehydes. In *Catalysis of Organic Reactions*; Malz, R. E., Ed.; CRC Press: Boca Raton, FL, 1996; p 15.

(22) Fouilloux, P. In *Heterogeneous Catalysis and Fine Chemicals: Proceedings of an International Symposium*, Poitiers, France, March 15−17, 1988; Guisnet, M., Barrault, J., Bouchoule, C., Duprez, D., Montassier, C., Pérot, G., Eds.; Studies in Surface Science and Catalysis, Vol. 41; Elsevier, Amsterdam, 1988; p 123.

(23) Rao, R.; Dandekar, A.; Baker, R. T. K.; Vannice, M. A. Properties of Copper Chromite Catalysts in Hydrogenation Reactions. *J. Catal.* **1997**, *171*, 406.

(24) Dandekar, A.; Baker, R. T. K.; Vannice, M. A. Carbon-Supported Copper Catalysts: II. Crotonaldehyde Hydrogenation. *J. Catal.* **1999**, *184*, 421.

Received for review February 28, 2007
Revised manuscript received June 5, 2007
Accepted June 8, 2007

IE070305N